Nanocluster Formation and Stabilization Fundamental Studies. 2. Proton Sponge as an Effective H+ Scavenger and Expansion of the Anion Stabilization Ability Series

ARTICLE *in* LANGMUIR · SEPTEMBER 2002

Impact Factor: 4.46 · DOI: 10.1021/la020225i

2 AUTHORS, INCLUDING:

Saim Özkar
Middle East Technical University
298 PUBLICATIONS **5,192** CITATIONS

Nanocluster Formation and Stabilization Fundamental Studies. 2. Proton Sponge as an Effective H^+ Scavenger and Expansion of the Anion Stabilization Ability Series

Saim Özkar† and Richard G. Finke*,‡

Department of Chemistry, Colorado State University, Fort Collins, Colorado 80523, and Department of Chemistry, Middle East Technical University, 06531 Ankara, Turkey

Received March 6, 2002. In Final Form: June 14, 2002

The two main goals of the current work are: (i) to test the effects of Proton Sponge as a H^+ scavenger and (ii) to test and rank the relative efficacy of the anions (Y^-) listed below for their relative ability to allow the formation, stabilization (including isolability), high catalytic activity, and long catalytic lifetime in the following, more generalizable transition metal nanocluster formation reaction: $1.0[Bu_4N]_qY + 1.0[(1,5\text{-}COD)Ir(I)(CH_3CN)_2]BF_4 + 2.5H_2 \rightarrow 1.0$cyclooctane $+ 1/n\{[Bu_4N]_{nq}[Ir(0)_n{\cdot}Y]\} + H^+BF_4^- + 2CH_3CN$. The anions investigated, Y^-, are the tri-Nb(V)-substituted polyoxoanion $SiW_9Nb_3O_{40}^{7-}$, the tri-Ti(IV)-substituted polyoxoanion $([P_2W_{15}(TiOH)_3O_{\sim 59}]^{9-})_n$ ($n = 1$, 2), citrate trianion ($C_6H_5O_7^{3-}$), acetate (OAc^-), trimetaphosphate ($P_3O_9^{3-}$), chloride (Cl^-), and hydroxide (OH^-). The five criteria we developed recently (Özkar, S.; Finke, R. G. *J. Am. Chem. Soc.* **2002**, *124*, 5796) are used to determine the effects of Proton Sponge (in comparison to control experiments employing $Bu_4N^+OH^-$) and to rank the Y^- anions. The results reveal that Proton Sponge is an effective, weakly coordinating, and generally preferred Brønsted base in comparison to the more basic and more coordinating OH^-, at least for the formation and catalytic properties of Ir(0) nanoclusters in acetone with Bu_4N^+ and for other conditions examined. The results also yield an expanded *anion series* of the relative ability of anions to promote the kinetically controlled formation, stabilization, and good catalytic properties of Ir(0) nanoclusters in acetone with Bu_4N^+ cations: $P_2W_{15}Nb_3O_{62}^{9-} \sim [(P_2W_{15}Nb_3O_{61})_2O]^{16-} \sim SiW_9Nb_3O_{40}^{7-} \sim ([P_2W_{15}(TiOH)_3O_{\sim 59}]^{9-})_n$ ($n = 1$, 2) $> C_6H_5O_7^{3-} > [-CH_2-CH(CO_2^-)-]_n^{n-} \sim OAc^- \sim P_3O_9^{3-} \sim Cl^- \sim OH^-$. The essence of this series, the first of its kind, is: *Brønsted basic polyoxoanions > citrate*$^{3-}$ *> other common anions used in nanocluster syntheses*. The results allow three other (five total) conclusions, results that should assist others in picking the best anions for the formation and stabilization of their own transition metal nanoclusters.

Introduction

In a recent paper, five criteria were introduced by which anions, solvents, cations, and polymers could be ranked for their ability to allow the kinetically controlled formation, and then stabilization, of modern transition metal nanoclusters formed from the reduction of metal salts under H_2.[1] That work emphasized *anionic* stabilizers of nanoclusters to start because of the fundamental significance of *nanocluster surface-adsorbed anions* in stabilizing transition metal nanoclusters (see the discussion and the references on this point all provided in ref 1). That initial work also emphasized Ir(0) nanoclusters stabilized by the polyoxoanions $P_2W_{15}Nb_3O_{62}^{9-}$ or its Nb−O−Nb bridged anhydride ($[(P_2W_{15}Nb_3O_{61})_2O]^{16-}$) because of the established advantages of starting with these well-studied nanoclusters, advantages that include the following:[1] (a) their well-characterized nature;[2] (b) the high level of stabilization afforded by such κ^3−O (tridentate, $(O)_3$-donating) oxoanions;[3] (c) the high catalytic lifetimes observed for $P_2W_{15}Nb_3O_{62}^{9-}/[(P_2W_{15}Nb_3O_{61})_2O]^{16-}$ stabilized nanoclusters (record lifetimes for polyoxoanion-stabilized Rh(0) nanoclusters);[4] and (d) the ability of their stoichiometry of formation (eq 1) to be generalized to other anions[1] (as well as other solvents, cations, and polymeric stabilizers via work in progress).[5] In addition, a major advantage of the Ir(0) polyoxoanion-stabilized nanoclusters is their well-understood mechanism of formation[6] under H_2 consisting of slow, continuous nucleation ($A \rightarrow B$, rate constant k_1, where A is the $[(1,5\text{-}COD)Ir(I)(CH_3CN)_2]BF_4$ (precursor in eq 1) and B is Ir(0) on the nanocluster's surface) and then fast, autocatalytic surface growth atop the nanocluster's "living metal polymer"[6b] surface ($A + B \rightarrow 2B$, the kinetic definition of autocatalysis, rate constant k_2). No other transition metal nanocluster system's mechanism of formation is as well-understood; hence, only in these transition metal nanoclusters can the effects of anions, solvents, cations, polymers, and other additives on the *kinetics of nanocluster formation* be so quantitatively probed and understood.

Application of the methods and five criteria in our prior paper[1] allowed construction of an initial "anion series" of

* Corresponding author. Telephone: (970)491-2541. Fax: (970)-491-1801. E-mail: Rfinke@lamar.colostate.edu.

† Middle East Technical University.

‡ Colorado State University.

(1) Özkar, S.; Finke, R. G. *J. Am. Chem. Soc.*, **2002**, *124*, 5796.

(2) (a) Lin, Y.; Finke, R. G. *J. Am. Chem. Soc.* **1994**, *116*, 8335. (b) Lin, Y.; Finke, R. G. *Inorg. Chem.* **1994**, *33*, 4891.

(3) (a) That the C_{3v} symmetry $P_2W_{15}Nb_3O_{62}^{9-}$ polyoxoanion presents a chelating, C_{3v} symmetry triad of Nb−O oxygens for binding to metals is not an assumption but rather is known with certainty by X-ray crystallography on the complex[3b] $[(C_5Me_5)Rh{\cdot}P_2W_{15}Nb_3O_{62}]^{7-}$ and by ^{17}O NMR on the complex[3c] $[(1,5\text{-}COD)Ir{\cdot}P_2W_{15}Nb_3O_{62}]^{8-}$. (b) Pohl, M.; Lin, Y.; Weakley, T. J. R.; Nomiya, K.; Kaneko, M.; Weiner, H.; Finke, R. G. *Inorg. Chem.* **1995**, *34*, 767. (c) Pohl, M.; Finke, R. G. *Organometallics* **1993**, *12*, 1453.

(4) Aiken, J. D., III; Finke, R. G. *J. Am. Chem. Soc.* **1999**, *121*, 8803.

(5) Starkey, L.; Hornstein, B. J.; Finke, R. G. Unpublished work and experiments in progress.

(6) For an introduction to the mechanisms of transition metal nanocluster formation, including a comprehensive listing of the prior literature in the area, see: (a) Watzky, M. A.; Finke, R. G. *J. Am. Chem. Soc.* **1997**, *119*, 10382 and references therein. (b) Watzky, M. A.; Finke, R. G. *Chem. Mater.* **1997**, *9*, 3083. (c) Aiken, J. D., III; Finke, R. G. *J. Am. Chem. Soc.* **1998**, *120*, 9545 and references therein to diffusive agglomeration of nanoparticles. (d) Widegren, J. A.; Aiken, J. D., III; Özkar, S.; Finke, R. G. *Chem. Mater.* **2001**, *13*, 312 and references therein.

10.1021/la020225i CCC: $22.00
Published on Web 09/06/2002

the relative ability of a given anion to allow the kinetically controlled formation, and then stabilization including isolation, of modern transition metal nanoclusters according to the five criteria (and specifically for Ir(0) nanoclusters in acetone solvent with Bu_4N^+ countercations):[1] $[(P_2W_{15}Nb_3O_{61})_2O]^{16-}$ > $C_6H_5O_7^{3-}$ (citrate trianion) > $[-CH_2-CH(CO_2)-]_n^{n-}$ (polyacrylate) ~ Cl^-.

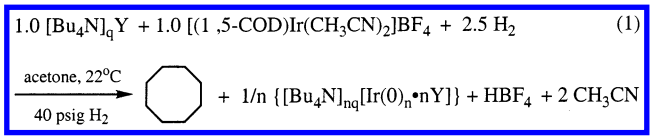

As part of our prior studies,[1] it was found that scavenging the 1.0 equiv of $H^+BF_4^-$ produced in eq 1 by adding 1.0 equiv of $Bu_4N^+OH^-$ led to important differences in the kinetics of nanocluster formation (as judged by its k_1 and k_2 rate constants and especially the diagnostic k_2/k_1 ratio, vide infra); effects on the resultant nanocluster's stability and catalytic lifetime were also observed.[1] The production of 1.0 equiv of H^+ is expected to influence nanocluster formation and stabilization[7] when one realizes that the resultant stabilizer of each anion tested in eq 1 (Y^-) is actually, therefore, *the conjugate acid* of that anion, H^+Y^-. However, if 1.0 equiv of $Bu_4N^+OH^-$ is added, then the much more Brønsted basic $Bu_4N^+Y^-$ is formed with the resultant (unprotonated) Y^- being able to coordinate to the Ir(0) surface (i.e., more so than H^+Y^-), thereby setting up the anionic electrostatic repulsion barrier around each nanocluster, a well-established, fundamental component of colloidal stabilization.[8] Noteworthy here is that the issue of H^+ formation and its scavenging is common to *all* nanocluster syntheses reducing metal cations under the common reductant, H_2; however, the effects of H^+ on nanocluster formation and stabilization are largely unstudied in modern nanocluster syntheses save our own earlier, brief studies on the effects of added[3a,6a] H^+ or OH^- and Bradley and co-worker's efforts on this topic.[7]

A subissue here is *the timing* of the addition of the 1.0 equiv of OH^-; ideally any such base would be added at the exact same rate as H^+ is formed in eq 1 so that excess OH^- would not be present and, therefore, unable to influence the >300 steps in the mechanism of formation of the ca. $Ir(0)_{\sim 300}$ nanoclusters that result in the case of the $P_2W_{15}Nb_3O_{62}^{9-}$/$[(P_2W_{15}Nb_3O_{61})_2O]^{16-}$ stabilizer.[6] Such a controlled OH^- addition at the exact rate of the H^+ formation reaction is, however, synthetically impractical—even if successful in one case with methods such as a syringe pump. The kinetic details change and thus would have to be worked out for each new anion, solvent, cation, polymer, or their combinations. In short, studying the effects of added bases, as well as finding a base that does not have unintended effects on the nanocluster formation steps, remained an important, unmet goal at the start of these studies.

Hence, two important questions were left unanswered by our initial studies: first, could a base be found that can be added at the start of the reaction and which will scavenge the H^+ as it is formed, but with minimal adverse effects on the nanocluster formation reaction—or perhaps even positive effects? On reflection, we hypothesized that sterically bulky, weakly coordinating, yet strongly Brønsted basic proton scavengers such as Proton Sponge might be just what is needed here (Proton Sponge = 1,8-bis-(dimethylamino)naphthalene). Hence, testing this "Proton Sponge hypothesis" became one of two main goals of the present work. The second goal of the present work is to test the relative efficacy of additional anionic stabilizers such as the Keggin-type polyoxoanions[9] $SiW_9Nb_3O_{40}^{7-}$ and the Ti(IV)-substituted Wells–Dawson type analogue $([P_2W_{15}(TiOH)_3O_{\sim 59}]^{9-})_n$, n = 1, 2;[10] such additional polyoxoanions being of special interest since the $[(P_2W_{15}Nb_3O_{61})_2O]^{16-}$ polyoxoanion had proven to be the best ("Gold Standard") stabilizer in our initial studies.[1] The readily available (but less Brønsted-basic) polyanion trimetaphosphate ($P_3O_9^{3-}$)[11] is another, simpler polyanion of fundamental interest to test since it, like the more complex polyoxoanions, presents a tridentate array of O atoms to the nanocluster's surface. The commonly used nanocluster stabilizer acetate ($CH_3CO_2^-$)[12] is an additional anion demanding testing, both because it is an often-used stabilizer and because it provides an interesting comparison point to polyacrylate ($[-CH_2-CH(CO_2^-)-]_n^{n-}$), a common polymeric stabilizer of nanoclusters. The interesting, previously unanswered question here is whether there is a discernible polymer/macromolecule effect due to the presence of the carboxylates within a single molecular chain, as in polyacrylate. Finally, it is also important to test simple hydroxide (OH^-) primarily as a control reaction to be sure that the above anionic bases or additives such as Proton Sponge are not functioning simply by deprotonating trace amounts of H_2O to form OH^- as the true nanocluster stabilizer. In short, the second goal of the present studies is to place the above anions in their correct relative positions within the developing anion series.

Herein we report the needed studies to answer the two goals outlined above. The results allow the important insights that Proton Sponge can be added at the start of the nanocluster formation reaction to scavenge the H^+ produced (eq 1) with positive effects in a number of cases on nanocluster kinetics of formation, stability, and catalytic lifetime. In addition, the other anions mentioned were successfully tested and ranked by the methods and five criteria, allowing an expanded anion series to be

(7) (a) Bradley and co-workers have published an important study showing that the synthesis of ~35 Å $Pt_{\sim 1500}$ nanoclusters under H_2 from $Pt^{IV}Cl_6^{2-}$ produces ~9000 equiv of H^+Cl^- and results in irreproducible catalytic activity of the nanoclusters varying by 670%. Significantly, however, when the excess H^+Cl^- is removed by dialysis, the catalytic activity both increased and became reproducible to ±15%. (b) Köhler, J. U.; Bradley, J. S. *Catal. Lett.* **1997**, *45*, 203.

(8) For a general discussion on the stability of colloids or nanoclusters see, for example: (a) Hirtzel, C. S.; Rajagopalan, R. *Colloidal Phenomena*: *Advanced Topics*; Noyes Publications: Park Ridge, NJ, 1985; pp 27–39, 73–87. (b) Hunter, R. J. *Foundations of Colloid Science*; Oxford University Press: New York, 1987; Vol. 1, pp 316–492. (c) Evans, D. F.; Wennerström, H. *The Colloidal Domain*, 2nd ed.; Wiley-VCH: New York, 1999. (d) See also the discussion and references provided in ref 1.

(9) (a) Finke, R. G.; Droege, M. W. *J. Am. Chem. Soc.* **1984**, *106*, 7274. (b) Finke, R. G.; Nomiya, K.; Green, C. A.; Droege, M. W. *Inorg. Synth.* **1992**, *29*, 239. (c) Lin, Y.; Nomiya, K.; Finke, R. G. *Inorg. Chem.* **1993**, *32*, 6040.

(10) (a) Nomiya, K.; Arai, Y.; Shimizu, Y.; Takahashi, M.; Takayama, T.; Weiner, H.; Nagata, T.; Widegren, J. A.; Finke, R. G. *Inorg. Chim. Acta* **2000**, *300–302*, 285–304. (b) Note that the Ti(IV)-substituted-$([P_2W_{15}(TiOH)_3O_{\sim 59}]^{9-})_n$, ($n$ = 1, 2) polyoxoanion proved so basic that even $Bu_4N^+OH^-$ is unable to deprotonate it or to completely cleave its final Ti–O–Ti anhydride linkage to yield its originally desired, more highly charged and thus potentially "super-stabilizing", "$P_2W_{15}Ti_3O_{62}^{12-}$" polyoxoanion with its "$[Ti^{IV}_3O_9]^{6-}$" site for attachment to the nanocluster's surface. Hence, the comparison of the tri-Ti(IV) versus tri-Nb(V) containing Wells–Dawson structure $P_2W_{15}M_3(OH)_xO_{62-x}^{n-}$ polyoxoanions (M = Nb(V), x = 0, n = 9; M = Ti(IV), x = 3, n also = 9) actually compares 3^- C_{3v} binding surfaces[3] with and without M–OH hydroxyl groups rather than $n = 9^-$ and 12^- polyoxoanions.

(11) (a) Day, V. W.; Klemperer, W. G.; Main, D. J. *Inorg. Chem.* **1990**, *29*, 2343 and references therein. (b) Oxidative reactions of the coordinated 1,5-COD ligand in $[(1,5\text{-COD})Ir\cdot P_3O_9]^{2-}$: Day, V. W.; Klemperer, W. G.; Lockledge, S. P.; Main, D. J. *J. Am. Chem. Soc.* **1990**, *112*, 2031.

(12) Reetz, M. T.; Maase, M. *Adv. Mater.* **1999**, *11*, 773.

determined: $P_2W_{15}Nb_3O_{62}^{9-} \sim [(P_2W_{15}Nb_3O_{61})_2O]^{16-} \sim SiW_9Nb_3O_{40}^{7-} \sim ([P_2W_{15}(TiOH)_3O_{\sim 59}]^{9-})_n$ (n = 1, 2) > $C_6H_5O_7^{3-}$ > $[-CH_2-CH(CO_2^-)-]_n^{n-} \sim OAc^- \sim P_3O_9^{3-} \sim Cl^- \sim OH^-$.

In other work in progress, we are successfully ranking the nanocluster formation and stabilization abilities of different solvents, cations, and polymeric additives and their combinations with the best anionic stabilizers. Those studies will be reported elsewhere in due course.[5]

Results and Discussion

Five Criteria. The five criteria developed previously and utilized to obtain the data in Table 1 are the relative ability of each nanocluster-stabilizing agent (i) to allow a high level of kinetic control in the formation of the nanoclusters, as judged quantitatively by the k_2/k_1 ratio;[1] the larger this ratio the better in the present case since there is more separation between nucleation and growth and, therefore, a higher level of kinetic control in the nanocluster formation reaction. (For more information on the use of the k_2/k_1 ratio, see the Supporting Information of ref 1.) The other criteria are the ability of each nanocluster-stabilizing agent (ii) to allow the formation of a near-monodisperse (≈ 15%) size distribution of nanoclusters (as judged by transmission electron microscopy (TEM) imaging and NIH Image counting of the nanoclusters), the narrower the distribution the better; (iii) to allow the nanoclusters to be isolable, "bottleable", and ideally, totally redissolvable in acetone without the formation of bulk metal; (iv) to permit a high level of catalytic activity for redissolved nanoclusters as measured by the rate of the prototype test reaction of cyclohexene hydrogenation; and (v) to permit a long catalytic lifetime for redissolved nanoclusters, as measured by the maximum number of total turnovers (TTOs) for cyclohexene hydrogenation, the higher the TTOs the better. Note that criteria i−iii are general, applying to nanocluster formation and isolation regardless of the application one might have in mind, while criteria iv and v emphasize catalysis as the end application.

Table 1 contains the data for eight anions, primarily the results according to the five criteria without and then with Proton Sponge (16 total entries in all). Note that columns 7−12 in Table 1 provide the primary data for criteria i−v, respectively. Note also that, as footnote e in Table 1 indicates, when any bulk metal is formed, the TTO value is necessarily an upper limit on the TTOs due to the soluble nanoclusters; hence, an entry for TTOs is necessarily omitted when more than a small amount bulk metal is formed. Columns 3 and 4 in Table 1 provide the induction period (t_{ind}) and slope of the linear part of the hydrogenation curve ($-d[H_2]/dt$) since these are visually easily obtained (i.e., without any curve fitting as needed to obtain k_1 and k_2) and since we have demonstrated in ref 6a the relationships $k_1 \alpha 1/t_{ind}$ and $k_2 \alpha -d[H_2]/dt$. That is, it is intuitively useful to be able to look at the nanocluster formation kinetic curves provide herein and to realize that sigmoidal curves (such as that in Figure 1) with longer induction periods (long t_{ind}, hence small k_1) and sharp, fast down turns (high $-d[H_2]/dt$ and thus high k_2) correspond to the desired high k_2/k_1 ratio, indicating a high level of kinetic control in the nanocluster formation reaction.[1]

Before examining the data in Table 1, it is also useful to note that we will be referring to Table S-1 of the Supporting Information since it contains entries for the effects of added $Bu_4N^+OH^-$ for most of the anions, data that have been relegated to the Supporting Information since 1. 0 equiv of added Proton Sponge provides equivalent results (in a few cases) to superior results (in several cases) in comparison to the addition of 1. 0 equiv of $Bu_4N^+OH^-$. Table S-1 also contains a compilation of all the data from both this study and our earlier work,[1] a compilation from which the absolute anion series is provided at the end of the paper for the 10 anions that we have examined to date.

Use of Proton Sponge as a H^+ Scavenger Resulting in a Comparison of the $P_2W_{15}Nb_3O_{62}^{9-}$ Polyoxoanion versus the Nb−O−Nb Bridged $[(P_2W_{15}Nb_3O_{61})_2O]^{16-}$ Polyoxoanion. Table 1, entry 1, lists the data collected for 1.2 mM $[(1,5\text{-COD})Ir(CH_3CN)_2]BF_4$ plus 1.2 mM $[Bu_4N]_9[P_2W_{15}Nb_3O_{62}]$ under what is hereafter designated as standard conditions (in acetone at 22 °C and 40 psig H_2 to start; see Experimental Section for further details). The key data in columns 7−12 in Table 1 are a needed comparison point for the studies herein; moreover, the data in Table 1, entry 1, are those for the previous best (Gold Standard)[1] anionic stabilizer examined to date, $[(P_2W_{15}Nb_3O_{61})_2O]^{16-}$. The data in entry 1 for this Gold Standard stabilizer show that the resultant nanoclusters form with a relatively high $k_2/k_1 = 1.9(2) \times 10^5$ M^{-1} and thus a high degree of kinetic control, and that a relatively narrow 21(4) Å (i.e., ±19%) distribution of nanoclusters results by TEM. In addition, the data in entry 1 for the $[(P_2W_{15}Nb_3O_{61})_2O]^{16-}$ stabilizer show that the supernatant of the resultant solution is clear and blue for reasons to be explained in a moment. (There is a well-established precipitation of some of the nanoclusters as the cyclohexene hydrogenation proceeds, producing the less polar cyclohexane, which in turn causes some of the salt-stabilized nanoclusters to precipitate.) The data in entry 2 also show, however, that that the nanoclusters are fully redissolvable in fresh acetone after they have been taken to dryness. Finally, the data in entry 1 of Table 1 reveal good catalytic activity (0.8(1) mmol of H_2/h) and nanocluster catalytic lifetime (51 000 TTOs) from the isolable, bottleable, $[(P_2W_{15}Nb_3O_{61})_2O]^{16-}$ polyoxoanion-stabilized nanoclusters.

As a control, the data in entry 1 of Table S-1 of the Supporting Information show that essentially the same results within experimental error are obtained if one makes Ir(0) nanoclusters under standard conditions starting with the *preformed, isolated complex* $[Bu_4N]_5Na_3[(1,5\text{-COD})Ir{\cdot}P_2W_{15}Nb_3O_{62}]$. The differences here are the slightly different, mixed Na^+/Bu_4N^+ versus all Bu_4N^+ countercation mixture plus the difference due to the $2CH_3CN$ and $1Bu_4N^+BF_4^-$ byproducts that are produced by the in situ method (eq 1 and entry 1, Table 1).

Note that the data in entry 1 of Table 1 (as well as entry 1, Table S-1) refer to the Nb−O−Nb bridged anhydride polyoxoanion ($[(P_2W_{15}Nb_3O_{61})_2O]^{16-}$) as the actual stabilizer since 1 equiv of H^+ leads, in the absence of added exogenous base, to protonation of the polyoxoanion, $HP_2W_{15}Nb_3O_{62}^{8-}$ (pK_a = ca. 9)[13] and then condensation of $2HP_2W_{15}Nb_3O_{62}^{8-}$ to give $1H_2O$ plus $1[(P_2W_{15}Nb_3O_{61})_2O]^{16-}$ (eq 2). This well-precedented sequence[2] is then followed by the also well-established[2] $2H_2$ reduction of 4W(VI) sites in $[(P_2W_{15}Nb_3O_{61})_2O]^{16-}$ to yield the 4W(V)-containing heteropolyblue form shown in eq 3.[14] This sequence reveals *another special function of polyanionic stabilizers* such as $P_2W_{15}Nb_3O_{62}^{9-}$; they are *multibasic anions* that can scavenge H^+ and self-buffer nanocluster formation reactions proceeding according to eq 1. (The protons in eq 3

(13) Weiner, H.; Aiken, J. D., III; Finke, R. G. *Inorg. Chem.* **1996**, *35*, 7905.

(14) Lead references to heteropolyblues include (a) Pope, M. T. *Heteropoly and Isopoly Oxometallates*; Springer-Verlag: Berlin, 1983. (b) Pope, M. T. In *Mixed-Valence Compounds*; Brown, D. B., Ed.; Reidel: Dordrecht, The Netherlands, 1980. (c) Buckley, R. L.; Clark, R. J. H. *Coord. Chem. Rev.* **1985**, *65*, 167.

Table 1. Compilation of Data for the Anionic Stabilizers

entry[a]	precursor	t_{ind} (h)	$(-d[H_2]/dt)$ (mmol of H_2/h)	k_1 (h^{-1})	$k_2 \times 10^{-3}$ ($M^{-1}\,h^{-1}$)[b]	$k_2/k_1 \times 10^{-5}$ (M^{-1})[b]	d_m (Å)	appearance	redispersibility	cat acty (mmol of H_2/h)	TTO
					$[P_2W_{15}Nb_3O_{62}]^{9-}$						
1	$[(COD)Ir(CH_3CN)_2]BF_4$ + $[Bu_4N]_9P_2W_{15}Nb_3O_{62}$	1.5(3)	1.7(2)	0.008(1)	1.5(1)	1.9(2)	21(4)	clear, blue[c]	yes	0.8(1)	51 000
2	$[Bu_4N]_5Na_3[(COD)Ir{\cdot}P_2W_{15}Nb_3O_{62}]$ + 1 equiv of Proton Sponge	0.7(1)	3.1(4)	0.008(1)	3.5(1)	4.4(5)	21(4)	clear, blue[c]	yes	2.2(2)	68 000
					$[SiW_9Nb_3O_{40}]^{7-}$						
3	$[Bu_4N]_4Na_2[(COD)Ir{\cdot}SiW_9Nb_3O_{40}]$	0.5(1)	3.6(4)	0.049(3)	3.7(1)	0.76(5)	22(4)	brown, slightly turbid[d]	part[d]	1.2(1)	57 000
4	$[Bu_4N]_4Na_2[(COD)Ir{\cdot}SiW_9Nb_3O_{40}]$ + 1 equiv of Proton Sponge	0.5(1)	3.8(4)	0.040(2)	4.7(1)	1.2(1)	21(4)	brown, slightly turbid[d]	part[d]	2.6(3)	41 000
					$\{[P_2W_{15}(TiOH)_3O_{59}]^{9-}\}_n$ (n = 1, 2)						
5	$[(COD)Ir(CH_3CN)_2]BF_4$ + $[Bu_4N]_{(8n+1)}[P_2W_{15}(TiOH)_3O_{59}]_n$	0.7(2)	4.5(4)	0.021(2)	4.1(1)	2.0(1)	22(3)	clear, deep blue[c]	yes	2.3(2)	29 000
6	$[(COD)Ir(CH_3CN)_2]BF_4$ + $[Bu_4N]_{(8n+1)}[P_2W_{15}(TiOH)_3O_{59}]_n$ + 1 equiv of Proton Sponge	1.0(2)	2.8(4)	0.009(1)	2.8(1)	3.1(3)	21(3)	clear, deep blue[c]	yes	0.7(1)	32 000
					$[C_6H_5O_7]^{3-}$						
7	$[(COD)Ir(CH_3CN)_2]BF_4$ + $[Bu_4N]_3C_6H_5O_7$	2.0(2)	1.8(2)	0.022(2)	1.1(1)	0.50(5)	23(5)	brown, black particles	part.	0.4(1)	[≤43 000][e]
8	$[(COD)Ir(CH_3CN)_2]BF_4$ + $[Bu_4N]_3C_6H_5O_7$ + 1 equiv of Proton Sponge	1.2(2)	4.4(4)	0.015(1)	2.0(1)	1.3(1)	18(4)	clear, brown	yes	0.4(1)	7 600
					$[C_2H_3O_2]^{-}$						
9	$[(COD)Ir(CH_3CN)_2]BF_4$ + $[Bu_4N]C_2H_3O_2$	0	4.5(4)	≥1.1(1)	0.20(2)	≤0.0018(2)][f]	17(5)	clear, brown	part.	0.9(2)	[≤81 000][e]
10	$[(COD)Ir(CH_3CN)_2]BF_4$ + $[Bu_4N]C_2H_3O_2$ + 1 equiv of Proton Sponge	0.1(1)	10(1)	≥1.1(1)	4.5(1)	≤0.041(4)][f]		brown, black particles	part.	2.0(2)	
					$[P_3O_9]^{3-}$						
11	$[(COD)Ir(CH_3CN)_2]BF_4$ + $[Bu_4N]_3[P_3O_9]$	1.0(2)	2.8(4)	0.021(2)	2.6(1)	1.2(1)		clear, black particles	no		[≤82 000][e]
					Cl^{-}						
12	$[(COD)Ir{\cdot}Cl]_2$	0.1(1)	12(1)	0.030(5)	11(1)	3.6(7)		clear, black particles	no		
13	$[(COD)Ir{\cdot}Cl]_2$ + 1 equiv of Proton Sponge	0	10(1)	≥0.88(5)	8.9(3)	[≤0.10(1)][f]		clear, black particles	no		
					OH^{-}						
14	$[(COD)Ir(CH_3CN)_2]BF_4$ + 0 equiv of Bu_4NOH	0	13(1)	≥1.3(2)	21(1)	[≤0.16(3)][f]		clear, black particles	no		
15	$[(COD)Ir(CH_3CN)_2]BF_4$ + 1 equiv of Bu_4NOH	0.2(1)	7.2(1)	0.51(5)	2.6(1)	0.051(5)		clear, black particles	no		
16	$[(COD)Ir(CH_3CN)_2]BF_4$ + 2 equiv of Bu_4NOH	~1	0.7(1)	0.039(1)	0.51(1)	0.13(1)		brown, black particles	part.	0.4(1)	

[a] The data in entry 2 are the average of three experiments; all the other entries are the average of two experiments, except when bulk metal was seen (and, then, the resulting experiment is, therefore, of less interest). [b] The k_2 values are corrected by the mathematically required stoichiometry factor of 1400 as detailed in ref 6a. [c] The blue color is due to the well-established formation of a two-electron reduced heteropolyblue because of reduction of two W(VI) in the polyoxoanion to two W(V). [d] Since the isolated nanoclusters are completely redissolvable in acetonitrile (a more polar solvent than acetone) the "slight turbidity" and "only partial redispersibility" in the case of these $SiW_9Nb_3O_{40}^{7-}$-stabilized nanoclusters is not due to bulk Ir(0) formation but rather reflects the lower solubility of $SiW_9Nb_3O_{40}^{7-}$ anion as its mixed Na^+/Bu_4N^+ salt. [e] Because of the formation of bulk metal, the values in [ ] are upper limits to the true nanoparticle TTOs. [f] The small to nonexistent induction period in these cases means that these k_2/k_1 values are expected to be less reliable and probably upper limits.

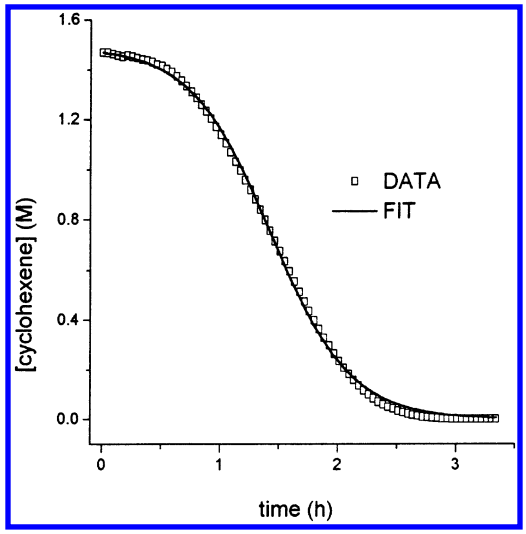

Figure 1. Cyclohexene loss vs time and curve-fit for the hydrogenation of 1.6 M cyclohexene and concomitant formation of 21 ± 4 Å Ir(0) nanoclusters starting with 1.2 mM $[Bu_4N]_5Na_3[(1,5\text{-COD})Ir{\cdot}P_2W_{15}Nb_3O_{62}]$ and 1.2 mM (1 equiv) Proton Sponge in acetone at 22 °C. A 0.7(1) h induction period is seen before the cyclohexene hydrogenation proceeds. The H_2 loss (uptake) data are what is actually collected; the pressure rise in the initial part of the curve (because of the solvent vapor pressure reequilibration after 15 flushes with H_2 before the reaction was started) is corrected as described in ref 6d (and, hence, is not seen in this or subsequent figures containing kinetic data). The data are then transformed into the cyclohexene loss data in units of M/s as required for the curve-fitting procedure; see the Experimental Section. Note that $-d[H_2]/dt = -d[\text{cyclohexene}]/dt$ is due to the 1:1 stoichiometric relationship between H_2 and cyclohexene.[6a] From that data the rate $-d[H_2]/dt = -d[\text{cyclohexene}]/dt = 3.1(4)$ mmol H_2/h listed in Table 1 was calculated from the maximum slope past the induction period. In both this figure and all later cyclohexene loss figures (including those in the Supporting Information), the rate constants for the slow, continuous nucleation (k_1) and autocatalytic surface-growth (k_2) listed in Table 1 were obtained from the nonlinear least squares curve-fit to the analytic equations[28a] for these two pseudo-elementary steps[6a] plus the pseudo-elementary hydrogenation reporter reaction[6a] eqs 2a–c, described in detail in ref 6a. The k_2 value has been corrected by the mathematically required 1400 stoichiometry factor,[6a] both here and in all the other k_2 entries in Table 1 and in the Supporting Information.

are bound to the 20^- charged polyoxoanion but are shown separately to emphasize their stoichiometry of formation concomitant with the formation of the heteropolyblue form of the polyoxoanion):

$$P_2W_{15}Nb_3O_{62}^{9-} + H^+ \rightarrow 0.5[(P_2W_{15}Nb_3O_{61})_2O]^{16-} + 0.5H_2O \quad (2)$$

$$0.5[(P_2W_{15}Nb_3O_{61})_2O]^{16-} + H_2 \rightarrow 0.5[(P_2W^{VI}{}_{13}W^{V}{}_2Nb_3O_{61})_2O]^{20-} + 2H^+ \quad (3)$$

On reflection, Proton Sponge ($pK_a = 12.3$)[15] seemed like an ideal strong base that is, however, sterically bulky and thus *poorly coordinating* so that it could be added *at the start* of a nanocluster formation reaction to scavenge H^+ and yet have minimal effects on the nanocluster formation steps of nucleation (k_1) and autocatalytic surface growth (k_2). In an otherwise standard conditions experiment starting with 1.2 mM of the preformed, isolated precursor

(15) (a) Brzezinski, B.; Schroeder, G.; Grech, E.; Malarski, Z.; Sobczyk, L. *J. Mol. Struct.* **1992**, *274*, 75. (b) Brzezinski, B.; Glowiak, T.; Grech, E.; Malarski, Z.; Sobczyk, L. *J. Chem. Soc., Perkin Trans.* **1991**, *2*, 1643.

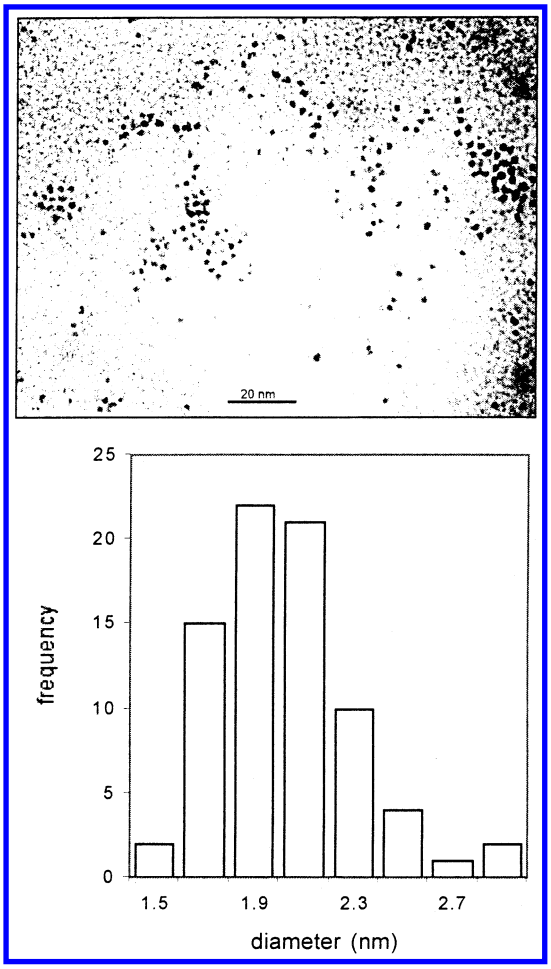

Figure 2. TEM image (430K magnification) and associated particle size histogram (79 nontouching particles counted by NIH Image) of isolated 21 ± 4 Å Ir(0) nanoclusters grown by hydrogen reduction of 1.2 mM $[Bu_4N]_5Na_3[(1,5\text{-COD})Ir{\cdot}P_2W_{15}Nb_3O_{62}]$ and 1.2 mM Proton Sponge in acetone under standard conditions. The sample was harvested after 14 h hydrogenation and, therefore, after complete formation of nanoclusters as proven by a cyclooctane evolution experiment (see eq 1) as described in the Experimental Section.

$[Bu_4N]_9Na_3[(1,5\text{-COD})Ir{\cdot}P_2W_{15}Nb_3O_{62}]$, 1.2 mM Proton Sponge was added at the start of the nanocluster formation reaction. A typical sigmoidal-shaped cyclohexene loss versus time curve is seen (Figure 1), one well-fit by the A → B and A + B → 2B equations and rate constants k_1 and k_2. Compared to the data in entry 1 without Proton Sponge (i.e., for the in situ, eq 1 prepared precatalyst), the data in entry 2 of Table 1 reveals a 2.3-fold larger k_2/k_1 value, a 2.8-fold higher catalytic activity, and a 1.3-fold higher TTOs value (Figure S-1 of the Supporting Information). The resultant solution is still completely redissolvable post-drying and still contains ca. 21(4) Å nanoclusters by TEM (Figure 2). A control experiment was also done obtaining the data for the preformed, isolated precursor $[Bu_4N]_9Na_3[(1,5\text{-COD})Ir{\cdot}P_2W_{15}Nb_3O_{62}]$ *without* Proton Sponge (entry 1, Table S-1) and so that it could be compared to entry 2, Table 1. This comparison shows an identical 2.3-fold larger k_2/k_1 value, a slightly smaller 1.2-fold higher catalytic activity, and a comparable 1.7-fold higher TTOs value—that is, this control shows that the effects of Proton Sponge are basically equivalent within experimental error regardless if one compares those effects to the preformed complex or the in situ prepared complex (eq 1) without Proton Sponge.

The invariance of the rate constant (k_1) without and with Proton Sponge in entries 1 and 2 in Table 1 (and in

entry 1, Table S-1) shows that Proton Sponge has no effect—and certainly no negative effect—within experimental error on the crucial nanocluster nucleation process.

Two molecular weight determination control experiments were also done verifying that the Nb−O−Nb bridged anhydride ($[(P_2W_{15}Nb_3O_{61})_2O]^{16-}$) is formed as expected[2] in the absence of added base (eqs 2 and 3), but that adding 1 equiv of Proton Sponge does prevent its formation and results instead, as desired, in the formation of monomeric $P_2W_{15}Nb_3O_{62}^{9-}$ as the stabilizing polyoxoanion. (See the ultracentrifugation solution molecular weight measurement provided in Figure S-1 in ref 1.)

In summary, the main findings to this point are the following: (i) Proton Sponge behaves as desired with generally positive effects on nanocluster formation, stabilization, and resultant catalytic properties; and (ii) the resultant, unprotonated anion ($P_2W_{15}Nb_3O_{62}^{9-}$) is slightly better than the previous "Gold Standard"[1] $[(P_2W_{15}Nb_3O_{61})_2O]^{16-}$ anion in its nanocluster formation and stabilization abilities. Given the anion series developed in ref 1 (of $[(P_2W_{15}Nb_3O_{61})_2O]^{16-}$ > $C_6H_5O_7^{3-}$ > $[-CH_2-CH(CO_2^-)-]_n^{n-} \sim Cl^-$), the expanded anion series to this point adds $P_2W_{15}Nb_3O_{62}^{9-}$ to the top of that series: $P_2W_{15}Nb_3O_{62}^{9-} \sim [(P_2W_{15}Nb_3O_{61})_2O]^{16-}$ > $C_6H_5O_7^{3-}$ > $[-CH_2-CH(CO_2^-)-]_n^{n-} \sim Cl^-$.

Other Polyoxoanions. *Keggin-Type Polyoxoanion,* $SiW_9Nb_3O_{40}^{7-}$. Our earlier work indicated that $SiW_9Nb_3O_{40}^{7-}$ (i.e., (1,5-COD)Ir·$SiW_9Nb_3O_{40}^{6-}$ plus H_2 under standard conditions) provides high kinetic control and close to near-monodisperse, 22 ± 4 Ir(0) nanoclusters.[2a] Hence, it is important to rank this anion for its nanocluster formation and stabilization abilities, including after Proton Sponge has been added. One issue to be aware of with $SiW_9Nb_3O_{40}^{7-}$ is that its structure allows a tri-Nb−O−Nb bridged (and thus more stable) anhydride form, $Si_2W_{18}Nb_6O_{77}^{8-}$ (i.e., $2SiW_9Nb_3O_{40}^{7-} + 6H^+ \rightarrow 3H_2O + Si_2W_{18}Nb_6O_{77}^{8-}$).[9] This polyoxoanion also presents a less basic as well as less symmetric C_s symmetry $[W_2Nb_1O_9]^-$ site[9] versus the C_{3v} trianionic $[Nb_3O_9]^{3-}$ site[9] in $P_2W_{15}Nb_3O_{62}^{9-}$ for coordinating to at least mono-metal complexes.

The results of two separate but otherwise standard conditions nanocluster synthesis and hydrogenation experiments, employing the precursor complex $(Bu_4N)_4Na_2$[(1,5-COD)Ir·$SiW_9Nb_3O_{40}$] without and then with 1 equiv of Proton Sponge, are listed in Table 1, entries 3 and 4. The sigmoidal-shaped and otherwise normal-looking cyclohexene loss versus time curves for the reactions with and without any added base can be seen in Figure S-2 of the Supporting Information along with the excellent curve fits to the nucleation and then autocatalytic surface growth mechanism. The comparison of the results for $SiW_9Nb_3O_{40}^{7-}$ without and with Proton Sponge to those for $P_2W_{15}Nb_3O_{62}^{9-}$ without and with Proton Sponge (entries 1 and 2 vs 3 and 4, Table 1) indicates that the $SiW_9Nb_3O_{40}^{7-}$ polyoxoanion is *almost as effective* as either the $P_2W_{15}Nb_3O_{62}^{9-}$ or $[(P_2W_{15}Nb_3O_{61})_2O]^{16-}$ polyoxoanion (differing in only its k_2/k_1 ratio, the k_2/k_1 value in entry 4 being 2.5-fold smaller than that in entry 1 and 3.6 smaller than the k_2/k_1 value in entry 2). Nicely formed nanoclusters result, 21(4) Å in the presence of Proton Sponge, for example, Figure S-3 of the Supporting Information. The slight turbidity seen in acetone solutions of these nanoclusters (columns 9 and 10 of entries 3 and 4, Table 1) is not due to bulk Ir(0) metal formation since clear solutions result in the more polar acetonitrile (footnote d of Table 1). This slight turbidity is due to the lower solubility of the Na^+ salt of its triply Nb−O−Nb bridged, $Si_2W_{18}Nb_6O_{77}^{8-}$ polyoxoanion, the species formed in entry 3 when no Proton Sponge has been added. The

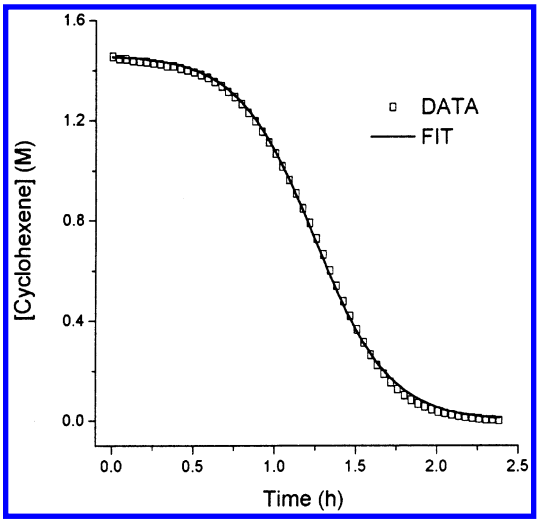

Figure 3. Cyclohexene loss vs time and curve-fit for the hydrogenation of 1.6 M cyclohexene and concomitant formation of near-monodisperse 22 ± 3 Å $Ir(0)_{\sim 300}$ nanoclusters starting with 1.2 mM $[Bu_4N]_{(8n+1)}[P_2W_{15}(TiOH)_3O_{59}]_n$ (based on its monomeric form) and 1.2 mM $[(1,5\text{-COD})Ir(CH_3CN)_2]BF_4$ in acetone at 22 °C. A 0.7(2) h induction period is seen, along with a maximum cyclohexene uptake of $-d[\text{cyclohexene}]/dt = -d[H_2]/dt = 4.5(4)$ mmol H_2/h. The rate constants for the nucleation and autocatalytic surface growth of the nanoclusters (k_1 and k_2, respectively) are provided in Table 1, entry 5.

data allow us to add $SiW_9Nb_3O_{40}^{7-}$ to the expanded anion series in a moment, but first it is useful to examine the data for the $([P_2W_{15}(TiOH)_3O_{\sim 59}]^{9-})_n$ polyoxoanion (entries 5 and 6 in Table 1) and then to compare both of these additional polyoxoanions to citrate (entries 7 and 8 in Table 1).

Wells−Dawson Type Polyoxoanion, $([P_2W_{15}(TiOH)_3O_{\sim 59}]^{9-})_n$, $n = 1, 2$. Among Wells−Dawson type polyoxoanions with their preferred high, C_{3v} symmetry and ^{31}P NMR handles, the most highly charged, *and thus potentially most highly nanocluster stabilizing,* Wells−Dawson type polyoxoanion available presently is the potentially super-basic "$P_2W_{15}Ti_3O_{62}^{12-}$".[10b] The issues here might be apparent to the reader: very strong, multiple $Ti^{IV}-O-Ti^{IV}$ anhydride bridge formation leading (in the tri-Ti^{IV}-substituted polyoxoanion) to a tetrameric composition and a multiply protonated polyoxoanion, $[H_{11}(P_2W_{15}Ti_3O_{(60.5)})_4]^{25-}$.[10a] Even with the very strong base Bu_4NOH, only partial deprotonation and partial cleavage of the four Ti−O−Ti bonds could be achieved. A mixture of the dimeric-like, monoanhydride-bridged $[H_6(P_2W_{15}Ti_3O_{61})_2O]^{16-}$ (plus some of the protonated monomer, $[H_3(P_2W_{15}Ti_3O_{62})]^{9-}$) proved (by ultracentrifugation MW measurements) to be the most highly charged, most basic form of this novel polyoxoanion available in solution.[10a] Nevertheless, it is of significant interest to use this $[H_6(P_2W_{15}Ti_3O_{61})_2O]^{16-}/[H_3(P_2W_{15}Ti_3O_{62})]^{9-}$ mixture (referred to in the title above, in Table 1, and hereafter as $([P_2W_{15}(TiOH)_3O_{\sim 59}]^{9-})_n$, $n = 1, 2$) to try to achieve even greater stabilization of the Ir(0) nanoclusters—is this highly charged polyoxoanion a "super stabilizer" or not?

In an otherwise standard conditions nanocluster synthesis and hydrogenation experiment, 1.2 mM $[(1,5\text{-COD})Ir(CH_3CN)_2]BF_4$ and 1.2 mM $(Bu_4N)_9[P_2W_{15}(TiOH)_3O_{\sim 59}]$ were employed; separate experiments were done without and then with 1 equiv of Proton Sponge (Table 1, entries 5 and 6) as well as with 1 equiv of Bu_4NOH (Table S-1, entry 9, of the Supporting Information). The sigmoidal-shaped and otherwise normal-looking cyclohexene loss versus time curve for the reaction without any added base is shown in Figure 3 along with the excellent curve fit (the

solid line) to the nucleation and then autocatalytic surface growth mechanism and its resultant k_1 and k_2 values. The similarly sigmoidal curve and curve fit in the presence of Proton Sponge is provided in Figure S-4 of the Supporting Information.

The key observables and results for the five criteria are listed in Table 1. In comparing data without Proton Sponge (entry 5 to entries 1 and 3) or with Proton Sponge (entry 6 to entries 2 and 4) it is clear that the values for the $([P_2W_{15}(TiOH)_3O_{\sim 59}]^{9-})_n$ polyoxoanion are in the general range of those for the $P_2W_{15}Nb_3O_{62}^{9-}$ and $SiW_9Nb_3O_{40}^{7-}$ polyoxoanions, yielding well-formed, near-monodisperse ($\pm \leq 15\%$) 21(3)−22(3) Å nanoclusters, respectively (Figure S-5 in the Supporting Information). A perusal of the results in Table 1, entries 5 and 6, and in comparison to those for $P_2W_{15}Nb_3O_{62}^{9-}$ (entries 1 and 2, Table 1) indicate that $([P_2W_{15}(TiOH)_3O_{\sim 59}]^{9-})_n$ ($n = 1$, 2) polyoxoanion is *as effective*, but not more so, than either $P_2W_{15}Nb_3O_{62}^{9-}$ or $[(P_2W_{15}Nb_3O_{61})_2O]^{16-}$). The one place that $([P_2W_{15}(TiOH)_3O_{\sim 59}]^{9-})_n$ ($n = 1$, 2) is less effective is in its 29 000−32 000 TTOs versus the 68 000 seen for the $P_2W_{15}Nb_3O_{62}^{9-}$ polyoxoanion in the presence of Proton Sponge (entry 2 vs entries 5−6, Table 1; the TTO curve for entry 5 is provided as Figure S-6 of the Supporting Information; it shows no unusual features). Overall, the data place the $([P_2W_{15}(TiOH)_3O_{\sim 59}]^{9-})_n$ polyoxoanion with the other polyoxoanions and at the top of the anion series: $P_2W_{15}Nb_3O_{62}^{9-} \sim [(P_2W_{15}Nb_3O_{61})_2O]^{16-} \sim SiW_9Nb_3O_{40}^{7-} \sim ([P_2W_{15}(TiOH)_3O_{\sim 59}]^{9-})_n$ ($n = 1$, 2).

Citrate Anion, $C_6H_5O_7^{3-}$. Citrate^{3-} was the previous Gold Standard stabilizer;[1] for this reason, citrate was examined carefully in our recent work both without and then with added $Bu_4N^+OH^-$.[1] Since it is a needed comparison point to the studies with Proton Sponge herein, entry 7 of Table 1 summarizes the data first reported in ref 1 for nanoclusters formed from 1.2 mM [(1,5-COD)-$Ir(CH_3CN)_2]BF_4$ and 1.2 mM $(Bu_4N^+)_3$[citrate^{3-}] under standard conditions; entry 12 of Table S-1 summarizes the data[1] for $(Bu_4N^+)_3$[citrate^{3-}] plus 1 equiv of $Bu_4N^+OH^-$. While the reader specifically interested in citrate as a stabilizer will want to study our earlier work[1] as well as that of Henglein and Giersig,[16] the key for the purposes of the present work is that citrate without added base gives relatively poor kinetic control in comparison to the other anions examined so far also without Proton Sponge (entry 7, Table 1, a k_2/k_1 ratio 1.5-, 3.8-, and 4.0-fold less than entries 3, 1, and 5, respectively, in Table 1). Significantly, bulk metal and only partially redissolvable nanoclusters result with citrate without added base (entry 7, columns 9−10, Table 1). The 43 000 TTOs seen (column 12 of entry 7) are an upper limit to the TTOs of the *nanoclusters present* because of the presence of bulk metal and its contribution to the TTO value, as footnote e of Table 1 notes.

The addition of 1 equiv Proton Sponge is rather successful in the case of citrate (entry 8, Table 1) in that a clear-brown solution results yielding nanoclusters that are fully isolable and redissolvable (cf. entry 7, Table 1)—that is, *the resultant stabilization provided by citrate appears to be significantly improved by the addition of 1.0 equiv of Proton Sponge* and its scavenging of H^+. However, as the data in Table 1, entry 8, and the cyclohexene loss curve in Figure 4 show, with Proton Sponge the citrate-stabilized nanoclusters are still formed with an apparent ca. 4-fold lower level of kinetic control ($k_2/k_1 = 1.3(1) \times 10^5$ M^{-1}) as compared to the analogous $P_2W_{15}Nb_3O_{62}^{9-}$ polyoxoanion value ($k_2/k_1 = 4.4(5) \times 10^5$ M^{-1}) (Table 1, entries 8 vs 2). The poorer fit of the calculated curve in Figure 4 at longer times is suggestive of agglomeration of the citrate^{3-}-stabilized nanoclusters.

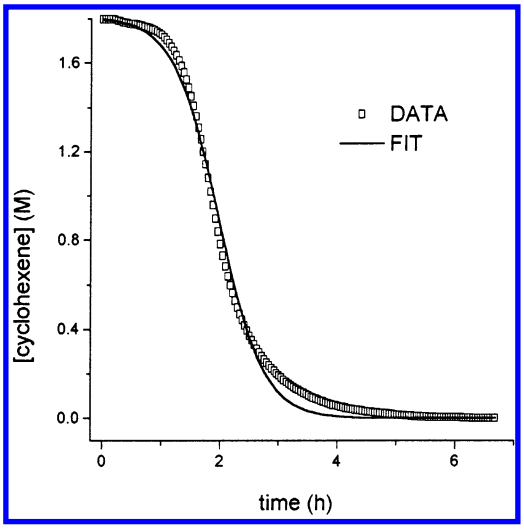

Figure 4. Cyclohexene loss vs time and curve-fit for the hydrogenation of 1.6 M cyclohexene and concomitant formation of 18 ± 4 Å Ir(0) nanoclusters starting with 1.2 mM $[Bu_4N]_3[C_6H_5O_7]$, 1.2 mM $[(1,5\text{-COD})Ir(CH_3CN)_2]BF_4$, and 1.2 mM (1 equiv) of Proton Sponge in acetone at 22 °C. A 1.2(2) h induction period is seen, along with a maximum cyclohexene uptake of $-d[\text{cyclohexene}]/dt = -d[H_2]/dt = 4.4(4)$ mmol H_2/h. The rate constants for the nucleation and the autocatalytic surface-growth of the nanoclusters are provided in Table 1, entry 8.

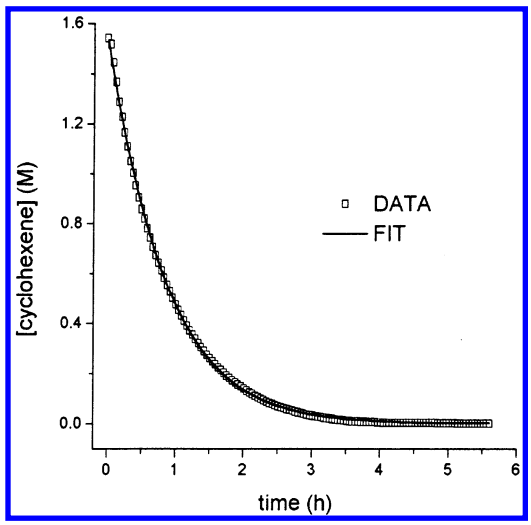

Figure 5. Cyclohexene loss vs time and curve-fit for the hydrogenation of 1.6 M cyclohexene and concomitant nanocluster formation starting with 1.2 mM $[Bu_4N][C_2H_3O_2]$ and 1.2 mM $[(1,5\text{-COD})Ir(CH_3CN)_2]BF_4$ in acetone at 22 °C. The cyclohexene uptake of $-d[\text{cyclohexene}]/dt = -d[H_2]/dt = 4.5(4)$ mmol H_2/h proceeds with no induction period. The rate constants for the nucleation and the autocatalytic surface growth of the nanoclusters are provided in Table 1, entry 10.

Also, a somewhat broader than near monodisperse distribution of nanoclusters results (18 ± 4 Å; ±22%; Figure S-7 of the Supporting Information), nanoclusters with a nearly order of magnitude lower catalytic lifetime (7600 TTOs, entry 8, Table 1 and Figure S-8 of the Supporting Information) than that observed for the $P_2W_{15}Nb_3O_{62}^{9-}$ polyoxoanion plus Proton Sponge case (68 000 TTOs; entry 2, Table 1). The lower k_2/k_1 value, broader dispersity, lower catalytic activity once redispersed, and lower TTOs *imply a lower effectiveness of citrate*$^{3-}$ in comparison to the formation and stabilization provided by $P_2W_{15}Nb_3O_{62}^{9-}$. Hence, at least for Ir(0)

(16) Henglein, A.; Giersig, M. *J. Phys. Chem. B* **2000**, *104*, 6767.

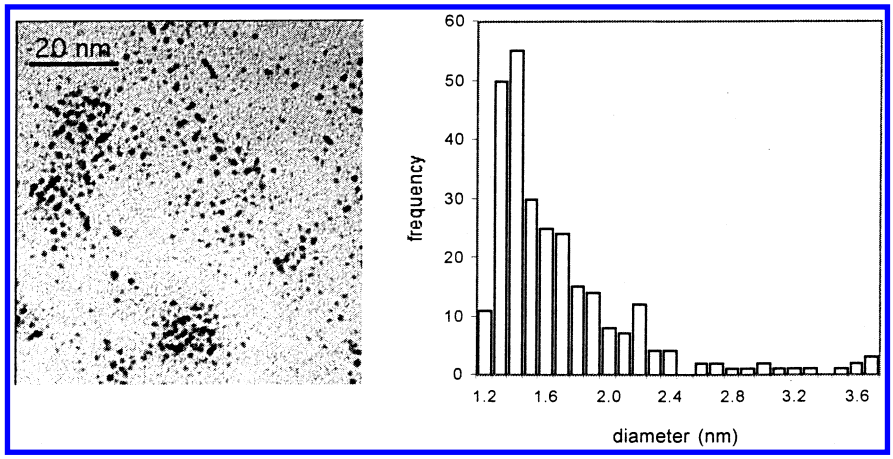

Figure 6. TEM image (430K magnification) and associated particle size histogram (309 nontouching particles counted by NIH Image) of isolated 17 ± 5 Å Ir(0) nanoclusters grown by hydrogen reduction of 1.2 mM [(1,5-COD)Ir(CH_3CN)$_2$]BF_4 with 1.2 [Bu_4N]-[$C_2H_3O_2$] in acetone under standard conditions described in the Experimental Section. This sample was harvested after 7 h.

nanoclusters in acetone and with Bu_4N^+ as the countercation, citrate is rated as below the polyoxoanions, the expanded anion series being: $P_2W_{15}Nb_3O_{62}^{9-} \sim [(P_2W_{15}Nb_3O_{61})_2O]^{16-} \sim SiW_9Nb_3O_{40}^{7-} \sim ([P_2W_{15}(TiOH)_3O_{\sim 59}]^{9-})_n$ (n = 1, 2) > $C_6H_5O_7^{3-}$.

Acetate Anion, $C_2H_3O_2^-$. Acetate is another commonly used nanocluster stabilizing anion;[12] however, the relative efficacy of acetate for nanocluster syntheses, stability, and catalysis had not been tested previously in any rigorous way. Significantly, no discernible induction period is seen in the cyclohexene loss versus time plot (Figure 5) when beginning with 1.2 mM [Bu_4N][OAc] and 1.2 mM [(1,5-COD)Ir(CH_3CN)$_2$]BF_4 in acetone at 22 °C. The implied *very low level of kinetic control* in the synthesis is indicated by an upper limit on $k_2/k_1 \leq 1.8(2) \times 10^2$ (Table 1, entry 9), *a value 10^3 smaller* than for the polyoxoanions or citrate^{3-}. The much larger $k_1 \geq 1.1(1)$ h^{-1} and smaller k_2/k_1 imply that the resultant nanoclusters should be smaller with a broader size distribution,[1] and the TEM data and resultant nanocluster distribution histogram (Figure 6) confirm this (17 ± 5 Å; ±30%) even when particles touching others (typically the larger particles) are ignored in the particle counting using NIH Image. Even a cursory look at the histogram in Figure 6 *reveals a large amount of tailing with its implied significant level of agglomeration of the nanoclusters because of inadequate stabilization by acetate.* Although no precipitation of bulk metal is observed in the clear-brown solution after 7 h hydrogenation, the isolated OAc^--stabilized nanoclusters are only partly redispersable in acetone and give a TTO value that is high, but unreliable, because of the presence of bulk metal (Figure S-9 of the Supporting Information).

The addition of 1 equiv of Proton Sponge does improve the k_2/k_1 ratio and hence the level of kinetic control in the nanocluster reaction by a factor of 23 (entry 10, Table 1, and Figure S-10 of the Supporting Information in comparison to entry 9, Table 1). Proton Sponge is 15-fold more effective in this regard than 1 equiv of Bu_4NOH (entry 15, Table S-1, and Figures S-11 (the kinetic curve) and S-12 (the TEM data) of the Supporting Information)—although in both cases there is little induction period, a situation that suggests little kinetic control in the nanocluster formation reaction. Overall (in both cases in Table 1, entries 9 and 10), OAc^- provides relatively little kinetic control, exhibiting k_2/k_1 values that are *1000−100-fold less* than that seen for the $P_2W_{15}Nb_3O_{62}^{9-}$ polyoxoanion (entries 9 and 10 vs entries 1 and 2, Table 1, respectively). The stabilization is poor as well; black bulk Ir(0) precipitates, and only partially redispersible nanoparticles result when using OAc^- either with or without Proton Sponge.

One question of interest here is how OAc^- compares to polyacrylate, $[-CH_2-CH(CO_2^-)-]_n^{n-}$. That is, is there a polymer/macromolecule effect of some type on Ir(0) nanocluster formation and stabilization? The needed polyacrylate data were obtained as part of our earlier studies[1] and are summarized as entries 17 and 18 of Table S-1 of the Supporting Information for the present paper. The key comparison is probably OAc^- plus 1 equiv of Proton Sponge (entry 10, Table 1, and also entry 16, Table S-1) versus 5 equiv of polyacrylate $[-CH_2-CH(CO_2^-)-]_n^{n-}$ of molecular weight 2000 (entry 18, Table S-1; the 5 equiv means 5 polyacrylate $-CO_2^-$ groups per [(1,5-COD)Ir-(CH_3CN)$_2$]BF_4 initially present). In both cases the level of kinetic control as judged by the k_2/k_1 ratios are similar (0.041(4) × 10^5 M^{-1} for OAc^- vs 0.032(3) × 10^5 M^{-1} for 5 equiv of polyacrylate), and only partially redissolvable nanoclusters result in each case. Hence, at least for the present studies (Ir(0) nanoclusters in acetone and with Bu_4N^+ countercations), there are no discernible polymer/macromolecule effects for the relatively small, 2000 molecular weight poly(acrylic acid) employed (we are examining other, higher molecular weight polymers in other work in progress).[5]

The results place OAc^- below citrate in the developing anion series and alongside polyacrylate: $P_2W_{15}Nb_3O_{62}^{9-} \sim [(P_2W_{15}Nb_3O_{61})_2O]^{16-} \sim SiW_9Nb_3O_{40}^{7-} \sim ([P_2W_{15}(TiOH)_3O_{\sim 59}]^{9-})_n$ (n = 1, 2) > $C_6H_5O_7^{3-}$ > $[-CH_2-CH(CO_2^-)-]_n^{n-} \sim OAc^-$. The finding that acetate anion is not nearly as good a stabilizer as its common use suggests is another significant finding from the present work.

Three Additional Anions: Trimetaphosphate ($P_3O_9^{3-}$), Chloride (Cl^-), and Hydroxide (OH^-). The results for these final three anions can be summarized briefly since, in the final analysis, none provided sufficient stabilization for isolable Ir(0) nanoparticles. Trimetaphosphate ($P_3O_9^{3-}$) did yield quite good kinetic control with a k_2/k_1 value of 1.2(1) × 10^5 M^{-1} (entry 11, Table 1, and Figure S-13 of the Supporting Information) as does Cl^- with its high k_2/k_1 value of 3.6(7) × 10^5 M^{-1} (entry 12, Table 1; see also Figure 8 given originally in ref 1 along with the discussion of the acetone hydrogenation that occurs in the case of entry 12 because of the formation of unscavenged H^+Cl^-).[1] *However*, in neither case did isolable and then redissolvable nanoclusters result. (The results for $P_3O_9^{3-}$ were checked as a control using the preformed, isolated, and purified [(1,5-COD)Ir·P_3O_9]$^{2-}$

complex to generate the nanoclusters;[17] again, nanoclusters that were not completely redissolvable were obtained.) In the case of Cl^-, the results were checked by the addition of 1 equiv of Proton Sponge (entry 13 of Table 1 and Figure S-14 of the Supporting Information), but no improvement in the nanocluster isolability was seen.

Finally, three separate controls were done with 1.2 mM $[(1,5\text{-COD})Ir(CH_3CN)_2]BF_4$ plus 0, 1, and 2 equiv of $Bu_4N^+OH^-$ under standard conditions in acetone at 22 °C (entries 14−16 and Figure S-15 of the Supporting Information). Only in the case of 2 equiv of $Bu_4N^+OH^-$ did some level of kinetic control result (entry 16; albeit a k_2/k_1 value 15-fold less than that in entry 1, Table 1), but only partially redissolvable nanoclusters resulted. The data are definitive in confirming[2a] that the added best stabilizers in Table 1 such as the polyoxoanions *do not* function by simply reacting with adventitious water to produce OH^- as the true stabilizer.

The results place $P_3O_9^{3-}$, Cl^-, and OH^- alongside OAc^- in the expanded anion series, better in some aspects (their kinetic control) but worse in others (the isolability of the resultant nanoclusters) as compared to OAc^-; that is $C_6H_5O_7^{3-} > [-CH_2-CH(CO_2^-)-]_n^{n-} \sim OAc^- \sim P_3O_9^{3-} \sim Cl^- \sim OH^-$.

Full Table of Data for All the Anions Investigated To Date. A full table comparing all the data for each anion examined either herein or before[1] is available as Table S-1 of the Supporting Information. While most of the main points contained within Table S-1 have already been discussed, a few additional points deserve mention. First, examination of the data comparing Proton Sponge versus $Bu_4N^+OH^-$ as the added base reveals that Proton Sponge gives a higher k_2/k_1 ratio and thus superior kinetic control in two cases (entries 12 vs 13 and entries 15 vs 16 in Table S-1) and no discernible difference in two others (entries 4 vs 5 and entries 9 vs 10 in Table S-1; the k_2/k_1 data in entries 21 and 22 for Cl^- is deemed less reliable because of the high uncertainty in the k_1 value). Second, comparing the Proton Sponge versus $Bu_4N^+OH^-$ for nanocluster isolability then redispersibility, catalytic activity, and TTOs catalytic lifetime data, there is a significant improvement using Proton Sponge for the $P_2W_{15}Nb_3O_{62}^{9-}$ case (entries 3 and 4 vs 5, Table S-1), whereas added $Bu_4N^+OH^-$ has a decidedly negative effect (comparing columns 9−12 in entries 3 and 4 to those for entries 1 and 2, Table S-1). However, there is probably little difference that is beyond the true experimental error for the cases in entries 9 versus 10 or entries 12 versus 13 in Table S-1. In short, Proton Sponge emerges as an effective, Brønsted basic, weakly coordinating, and hence generally preferred base in comparison to the more basic and more coordinating OH^-, at least for the Ir(0) nanoclusters and acetone with Bu_4N^+ and for the other conditions examined.

The results presented in the current work and those provided earlier (all of which are summarized in Table S-1) yield an expanded anion series for the first time: $P_2W_{15}Nb_3O_{62}^{9-} \sim [(P_2W_{15}Nb_3O_{61})_2O]^{16-} \sim SiW_9Nb_3O_{40}^{7-} \sim ([P_2W_{15}(TiOH)_3O_{\sim 59}]^{9-})_n$ (n = 1, 2) > $C_6H_5O_7^{3-} > [-CH_2-CH(CO_2^-)-]_n^{n-} \sim OAc^- \sim P_3O_9^{3-} \sim Cl^- \sim OH^-$. The essence of this final series is the following: *Brønsted basic polyoxoanions > citrate^{3-} > other common anions used in nanocluster syntheses*.

(17) A standard conditions nanocluster synthesis and hydrogenation experiment, using the known complex[11] $(Bu_4N)_2[(1,5\text{-COD})Ir{\cdot}P_3O_9]$ as precursor and under otherwise similar conditions, was done. Although nanocluster formation is slow (as judged by a ~20% cyclooctane evolution over ~30 h), bulk metal particles were again formed just as observed in the in situ generation experiment.

Summary and Conclusions

The following are the main conclusions from this work: (1) The significance of eq 1 and the H^+ produced, and thus the need to scavenge this H^+ with bases that have either minimal or positive effects on nanocluster formation and stabilization, were emphasized, an important but often overlooked aspect of transition metal nanocluster formations under H_2.

(2) The strongly basic but weakly coordinating base, Proton Sponge, was shown to be an effective scavenger of the H^+ byproduct of nanocluster formation (eq 1) while also having generally positive effects on the nanocluster nucleation and formation steps.

(3) Using the five criteria and methods herein, the expanded anion series provided above was obtained, the essence of which is the following: Brønsted-basic polyoxoanions > citrate^{3-} > other common anions used in nanocluster syntheses. As discussed in ref 1, this anion series refers rigorously only to the Ir(0) nanoclusters in acetone and with Bu_4N^+ for which it was measured. No *absolute* anion series is anticipated; for example, Pd is a metal that *appears* to be well-stabilized by Cl^- or OAc^- in combination with polymeric stabilizers.[18] Further studies of additional metals, anions, solvent, cations, and polymeric stabilizers are needed for $Ir(0)_n$ nanoclusters as well as for other $M(0)_n$ nanoclusters such as $Pd(0)_n$. Such studies are in progress[5] and will test the broader applicability of this first, guiding, nanocluster-stabilizing anion series. In addition, the number of Bu_4N^+ is not constant in the anion series (e.g., the $P_2W_{15}Nb_3O_{62}^{9-}$ polyoxoanion carries with it nine Bu_4N^+ while Cl^- carries only one), so that some stabilizing effect due to the cations seems probable and remains to be deconvoluted from the above anion stabilizer series via experiments in progress. We believe it is quite likely, however, that at least the key features of this first anion series will prove more generally applicable. (4) Brønsted-basic polyoxoanions, and especially the $P_2W_{15}Nb_3O_{62}^{9-}$ polyoxoanion with 1 equiv of Proton Sponge, are identified as the present "Gold Standard" stabilizing anions, at least for Ir(0) nanoclusters in acetone with Bu_4N^+ countercations. The main significance of this finding is that it provides a much-needed *reference point* for efforts to develop even better nanocluster stablizers. (5) A final important finding from this work is that the two best classes of stabilizers, namely, Brønsted-basic polyoxoanions and citrate^{3-}, each *present a facial array of three oxygens* for potential coordination to and stabilization of the nanoclusters. This novel observation has, in turn, led to the first detailed structural model for how such best stabilizing anions stabilize nanoclusters, a hypothesis that includes generalized predictions about which anions will be best for other transition metals. If that hypothesis stands up to further experimental scrutiny, then it promises to expedite the development of effective, tridentate stabilizers composed

(18) (a) Poorly compositionally characterized Pd nanoparticles stablized by Cl^-, possibly O (due to O_2 exposure), plus poly(*N*-vinyl-2-pyrrolidinone) (PVP) or polystyrene-*b*-poly(sodium)acrylate that do Suzuki coupling at 100 °C for 24 h: Li, Y.; El-Sayed, M. A. *J. Phys. Chem. B* **2001**, *105*, 8938. (b) Pd nanoclusters stabilized by OAc^- and polystyrene-*b*-poly-4-vinylpyridine block copolymers that appear to be stable and catalytically active for Heck coupling reactions at 140 °C for 3 days: Klingrlhöfer, S.; Heitz, W.; Greiner, A.; Oestreich, S.; Födster, S. Antonietti, M. *J. Am. Chem. Soc.* **1997**, *119*, 10116. (c) Pd nanos stabilized by Cl^-/OAc^- and propylene carbonate that are stable at 140−155 °C and do Heck coupling catalysis at those temperatures, but which cannot be isolated without bulk Pd formation upon removal of the solvent: Reetz, M. T.; Lohmer, G. *Chem. Commun.* **1996**, 1921.

of coordinating atoms other than oxygen,[19] a little investigated area.

Experimental Section

Materials. The source of all materials and any pretreatments employed are *identical* to this same section of ref 1. One note of emphasis from that section of ref 1 is that acetone was purchased from Burdick & Jackson (water content <0.2%) and was then purged with argon and transferred into a nitrogen atmosphere drybox before use. It is known that the source, purity, age, and H_2O content of the acetone all matter for reproducible nanocluster syntheses.[2b] Solutions of either Proton Sponge (Aldrich) or Bu_4NOH in acetone were made up fresh and should not stand for long periods of time because of aldol condensation reactions and different, enhanced catalytic rates from older solutions that we have seen in earlier work (see Table B and Figure G in the Supporting Information in ref 2b). The iridium solvate complex ($[(1,5\text{-COD})Ir(NCCH_3)_2]BF_4$) was prepared according to the procedure for the corresponding hexafluorophosphate salt[11a] and stored in the drybox. The nanocluster precursor complexes $[Bu_4N]_5Na_3[(1,5\text{-COD})Ir{\cdot}P_2W_{15}Nb_3O_{62}]$[20] and $[Bu_4N]_9[P_2W_{15}Nb_3O_{62}]$ were made by our most recent method;[13,21] $[Bu_4N]_4Na_2[(1,5\text{-COD})Ir{\cdot}SiW_9Nb_3O_{40}]$[9] was prepared from $[Bu_4N]_7[SiW_9Nb_3O_{40}]$[9], and $[Bu_4N]_{8n+1}[P_2W_{15}Ti_3(OH)_3O_{60-n}]_n$ ($n = 1-2$) was prepared by deprotonating the anhydride polyoxoanion $\{[Bu_4N]_{15}H_{17}[P_2W_{15}Ti_3O_{61.3}]_3\}$ with tetrabutylammonium hydroxide in acetonitrile solution.[10a] The purity of each of these complexes was checked by ^1H, ^{13}C, and ^{31}P NMR spectroscopy and then maintained by their storage in a drybox.

Hydrogenations. All the nanocluster formation and hydrogenation reactions were carried out on the previously described,[2a,6a] custom-built pressurized hydrogenation apparatus. Full details are reported in the Supporting Information of ref 1 under the heading Hydrogenations.

Curve Fits of the Hydrogen Uptake Data and Data Handling. Data handling and curve fitting of the H_2 pressure (or, equivalently, the cyclohexene loss) versus time data were performed, as described previously,[6d] using the software package Microcal Origin 3.5.4, which is a nonlinear regression subroutine (RLIN) and uses a modified Levenberg−Macquardt algorithm.[22] Error bars are typically ±15−20% unless specified otherwise (e.g., the somewhat larger error we have come to expect in k_1; see footnote 50 of ref 1); the error bars are not shown in the figures to avoid cluttering them.

TEM Sample Preparation. The solutions used for the TEM experiments were the exact same ones prepared below in the standard conditions and in the Catalytic Lifetime Experiments section (found in the Supporting Information). However, at the end of a given run (i.e., at a minimum time required for the complete formation of nanoclusters as determined by the cyclooctane evolution in the standard conditions hydrogenation) and at the end of the catalytic lifetime experiments, the Fischer−Porter (F−P) reaction bottle was detached from the hydrogenation line via its quick-connects and taken back into the drybox; its acetone solution was then transferred with a disposable polyethylene pipet into a clean, 5 mL screw-capped glass vial. The solution was dried under vacuum and the glass vial was then sealed and brought out of the drybox. The dry nanocluster samples were sent as solids in screw-capped glass vials to the University of Oregon for TEM investigation. There, 1 mL of acetonitrile was added in air just before a TEM was obtained to yield a clear amber, homogeneous solution (in general, no bulk metal was visible by the naked eye at any time unless otherwise indicated). A drop of this solution was then dispersed on a chloroform cleaned, carbon-coated Cu TEM grid.

TEM Analyses. TEM analyses were performed as before[2b,6a] at the University of Oregon with expert assistance of Dr. Eric Schabtach, using a Philips CM-12 TEM with a 70 μm lens operating at 100 kV and with a 2.0 Å point-to-point resolution, as described in detail previously.[2a] Typically, TEM pictures of each sample were taken at three different magnifications (100, 200, and 430 K) to obtain information about the sample in general (100 K), plus a closer visualization of the clusters (430 K). A number of control experiments were done previously, controls which provided good evidence that the results are truly representative of the sample (i.e., save any crystallization in the electron beam) and that the sample is not otherwise perturbed by application of the TEM beam [e.g., controls showing that varying the sample spraying method (in air or under N_2) or depositing the sample as a drop and letting it dry did not change the results; controls showing that changing the beam voltage from 40 to 100 kV or that changing the exposure time (seconds vs minutes) did not change the images; other controls have been done as well].[2a]

Particle Size Measurements. Particle size analysis was performed using the public domain NIH Image 1.62 program (available on the Internet at http://rsb.info.nih.gov/NIH Image/). The following steps were taken to prepare the data for analysis: (i) a bright field TEM image was obtained with even illumination. Images were chosen to be as representative of the bulk sample as possible; (ii) the image was then scanned into a computer using a scanning camera (Lumina) for the negative and saved as TIFF file; and (iii) using Adobe PhotoShop 3.0, the contrast/brightness and channel curves were adjusted so that particles stand out clearly from the background. This is the most difficult for small particles, which inherently have less contrast. In NIH Image 1.62, after having set the scale and the threshold, the "analyze particles" feature was used to generate a table of particle areas and diameters (major and minor axes). This table was then exported into Microsoft Excel 98 where histograms, statistical analysis, and histogram plotting were performed. For each particle, the diameter was calculated from the area by assuming that the nanoclusters are spherical. Size distributions are quoted as the mean diameter ± the standard deviation.

Nanocluster Formation and Cyclohexene Hydrogenations (Standard Conditions). These experiments were performed by following closely our established protocol[2b,6a] and are *identical* to the standard conditions procedure we used in our earlier work.[1] In addition, detailed experimentals are provided in the Supporting Information.

General Procedure for Catalyst Lifetime Experiments. These were performed *identically* as detailed before (see corresponding section in Supporting Information of ref 1). In addition, detailed experimentals are provided in the Supporting Information.

Solution Molecular Weight Measurements. The details of the ultracentrifuge sedimentation-equilibrium molecular weight determinations of the form of the polyoxoanion present with and without added base are provided in the Supporting Information available in ref 1.

Acknowledgment. This work was supported by the Department of Energy, Office of Basic Energy Sciences, via DOE Grant FG06-089ER13998. S.Ö. thanks the Fulbright Foundation for granting him a Fulbright Scholar Fellowship. We are also indebted to Mr. Jason Widegren for performing the ultracentrifugation experiments reported herein and to him and Dr. Brooks J. Hornstein for help proofreading the manuscript.

Supporting Information Available: Full details of each experiment and catalyst lifetime experiments including 15 figures and 1 table. This material is available free of charge via the Internet at http://pubs.acs.org.

LA020225I

(19) Özkar, S.; Finke, R. G. Molecular Insights for How Preferred Oxoanions Bind to and Stabilize Transition Metal Nanoclusters: A Tridentate, C_3 Symmetry, Lattice Size-Matching Binding Model, Submitted for Publication.

(20) Pohl, M.; Lyon, D. K.; Mizuno, N.; Nomiya, K.; Finke, R. G. *Inorg. Chem*. **1995**, *34*, 1413.

(21) The $P_2W_{15}O_{56}^{12-}$ for the synthesis of the $P_2W_{15}Nb_3O_{62}^{9-}$ used herein was prepared by the improved procedure described in Hornstein, B. J.; Finke, R. G. *Inorg. Chem*. **2002**, *41*, 2720.

(22) Press, W. H.; Flannery, B. P.; Teukolsky, S. A.; Vetterling, W. T. *Numerical Recipes*; Cambridge University: Cambridge, 1989.